Energy Conversion and Management 168 (2018) 611–628

Contents lists available at ScienceDirect

Energy Conversion and Management

journal homepage: www.elsevier.com/locate/enconman

Design and comparison of direct and indirect cooling system for 25 MW solar power plant operated with supercritical CO_2 cycle

M. Monjurul Ehsan[a,*], Zhiqiang Guan[a], A.Y. Klimenko[a], Xurong Wang[b]

[a] The Queensland Geothermal Energy Centre of Excellence (QGECE), School of Mechanical and Mining Engineering, The University of Queensland, Brisbane, QLD 4072, Australia

[b] School of Energy and Power Engineering, Xi'an Jiaotong University, Xi'an, Shanxi 710049, People's Republic of China

ARTICLE INFO

Keywords:
Cooling tower
supercritical CO_2
Shell and tube
Heat transfer
Heat exchanger

ABSTRACT

A validated MATLAB code is developed to design a dry cooling unit for a 25 MW solar power plant operated with supercritical CO_2 (sCO_2) Brayton cycle. Both direct and indirect cooling systems are designed for the power plant and their performance are compared. For direct cooling system, air cooled heat exchanger unit is designed whereas for indirect cooling system, optimum size of shell and tube heat exchanger is selected addressing the retainment of shell side heat transfer correction factor within a reasonable limit. The nonlinear property variation of sCO_2 near the critical condition is reasonably well captured by the present code in both shell and tube and air cooled heat exchanger units. The comparative study of direct and indirect cooling system is performed for inlet sCO_2 temperature of 71 °C, operating pressure of 7.5 MPa and ambient air temperature from 15 °C to 40 °C. For the same heat rejection, indirect cooling system requires a much higher cooling tower. During high ambient temperature period, direct dry cooling system shows superior cooling performance in terms of lower sCO_2 outlet temperature compared to indirect cooling system.

1. Introduction

Supercritical CO_2 due to its unique transport properties, has been discovered as one of the efficient and environmentally benign refrigerant substitutes in refrigeration and air conditioning technologies. The newly applications of sCO_2 have been proposed in thermal power plants with closed loop Brayton cycles. The sCO_2 power cycles are believed to be the next generation power cycles due to the lower cost, higher thermal efficiency and simplified plant design in comparison with traditional superheated Rankine power cycles [1]. One of the key challenges associated with sCO_2 power cycles is the cooling of sCO_2 near the critical temperature and pressure. A reliable and well-designed cooling system is required for efficient and smooth operation of thermal power plant. In arid areas, natural draft dry cooling towers (NDDCT) are preferred over the wet coolers due to the insufficient water supply, environmental concern and the high maintenance and operation cost related to wet cooling.

The first ever closed loop Brayton cycle was proposed by Feher [2] in 1967, where the cycle was modified by the introduction of a pump to handle the high density of sCO_2 during the compression process instead of using a compressor. Dostal et al. [1] performed comparative study among various sCO_2 Brayton cycles and higher thermal efficiency of 47% was observed with recompression Brayton cycle. Besarati and Goswami [3] conducted the thermal assessment of four different sCO_2 Brayton cycle configurations among which recompression with partial cooling showed highest cycle thermal efficiency of 50%. Conboy et al. [4] performed small scale experimentation with recuperated sCO_2 Brayton cycle to investigate the influence of operating conditions on the cycle performance. Al-Sulaiman and Atif [5] investigated the performance of different sCO_2 Brayton cycle layouts integrated with solar power tower. The recompression Brayton cycle showed promising performance with a thermal efficiency of 52%. Dyreby et al. [6] performed modelling study, where dry cooling unit is employed in a recompression sCO_2 cycles for concentrated solar power (CSP) application. The cycle overall efficiency of 43% with compressor inlet temperature of 50 °C was achieved with sCO_2 Brayton cycle using air cooled heat exchanger unit [7]. Wang and He [8] optimized the solar power tower with molten salt as heat transfer fluid in a sCO_2 recompression Brayton cycle with reheating. Zhang et al. [9] worked on the design and optimization of the heat source on the performance of sCO_2 Rankine cycle by exploring the influence of thermal boundary condition. Milani et al. [10] performed optimization studies in terms of thermal efficiency, water demand and solar power compatibility among various sCO_2 Brayton cycle layouts integrated with concentrated solar

* Corresponding author.
E-mail address: m.ehsan@uqconnect.edu.au (M. Monjurul Ehsan).

https://doi.org/10.1016/j.enconman.2018.04.072
Received 9 February 2018; Received in revised form 19 April 2018; Accepted 19 April 2018

Nomenclature

A	area, m^2
C_p	specific heat, J/kg K
C_{Dts}	drag coefficient
d	diameter, m
f	friction factor
F_{Dts}	drag force, N
G	mass velocity, kg/s m^2
H	height, m
h	heat transfer coefficient, W/m^2 K
J	shell side heat transfer correction factor
k	thermal conductivity, W/m K
K	loss coefficient
l_{ts}	length of tower support, m
L_t	length of finned tube, m
m	mass flow rate, kg/s
n_{ts}	number of tower supports
n_r	number of tube rows
n_{tr}	effective number of tubes per row
P_f	fin pitch, m
P_t	transversal tube pitch, m
P_l	longitudinal tube pitch, m
P_d	diagonal tube Pitch, m
ΔP	pressure drop, N/m^2
Q	heat transfer rate, W
R	shell side pressure drop correction factor
T	temperature, °C or K
t_f	fin thickness (mean), m
t_{ft}	fin tip thickness, m

Greek symbols

ε	surface roughness, m
η	efficiency
μ	dynamic viscosity, kg/ms
ρ	density, kg/m^3
σ	area ratio

Dimensionless number

Fr_D	Froude number
Nu	Nusselt number
Pr	Prandtl number
Re	Reynolds number
R_y	characteristic Reynold number
J	Colburn factor

Subscripts

a	air side
ct	cooling tower
ctc	cooling tower contraction
cte	cooling tower expansion
cv	control volume
he	heat exchanger
i	inner; inlet
o	outer; outlet
lm	log mean temperature difference
pc	pseudocritical
RB	Robinson and Brigg correlation
r	root
s	supercritical; shell side
t	tube side
to	tower outlet
ts	tower support
w	wall temperature

power systems. Song et al. [11] performed the thermal assessment of sCO_2 Brayton cycle by enhancing the preheating process. Padilla et al. [12] employed dry cooling system to assess the thermal efficiency with various sCO_2 Brayton cycles. Recompression cycle with intercooling achieved the highest cycle efficiency of 55.2% with turbine inlet temperature of 850 °C.

Experiments performed to assess the thermal performance of a small natural draft dry cooling tower coupled with 1 MW concentrating solar thermal sCO_2 power cycle [13]. Numerical computation conducted to investigate the cooling performance of a NDDCT under cross wind condition and factors influencing the deterioration of the cooling performance were also reported [14]. Numerical analysis with CFD model used to evaluate the cooling performance of NDDCT by optimizing the water distribution in cross wind condition [15]. Several recent studies were performed to investigate the thermal performance of NDDCT under cross-wind condition [16–20]. Sadafi et al. [21] performed experimentation to precool the inlet air in a NDDCT. Yubiao Sun et al. [22] also conducted experimentation to enhance the cooling performance by spraying water droplets at the inlet of the tower. The influences of nozzle arrangement, injection height and injection direction on the cooling performance were also carried out [23]. Trabelsi et al. [24] analysed the performance of dry cooled solar power tower with molten salt as a working fluid. The overall system was optimized with various solar filed size, size of turbine and type of heat transfer fluid.

So far researchers have explored the potential of sCO_2 as a working fluid in various closed loop Brayton cycle configurations. Few studies have investigated the cycle performance coupled with dry cooling units. Dai et al. [25] recently performed the comparison of direct and indirect dry cooling system operating with sCO_2 Brayton cycle under various ambient temperatures. The study was performed with an existing NDDCT of 20 m height and the design of air cooled heat exchanger unit was not taken into consideration. In the present work, the design and comparison of direct and indirect dry cooling system in a natural draft dry cooling unit are performed. One dimensional MATLAB code is generated to design the natural draft dry cooling tower for both direct and indirect cooling systems. The novelty of the present work includes the detailed analysis of an air cooled heat exchanger unit and shell and tube heat exchanger operated with sCO_2. The design of heat exchangers is a great challenge since the working fluid is sCO_2 and conventional method is not sufficient to predict the heat transfer accurately. The present code is able to predict the exact heat transfer mechanism and pressure drop characteristics of sCO_2 working with shell and tube and air cooled heat exchanger unit.

2. Dry cooling system classification

In dry cooling system, fresh ambient air is used to cool the turbine exhaust and the cooling medium never gets in contact with the working fluid. Fig. 1. shows a direct dry cooling system, where sCO_2 after following expansion process through the turbine is sent to the recuperator to preheat the sCO_2 stream from the compressor outlet. The sCO_2 is cooled by exchanging heat to the airstream flowing across the bundles of finned tube heat exchanger unit in a NDDCT. However, the cooling potential of a direct system depends on the dry air bulb temperature.

In indirect dry cooling system shown in Fig. 2, the turbine exhaust after flowing through the recuperator is sent to the pre-cooler, where the heat from the sCO_2 is transferred to the cooling water by shell and

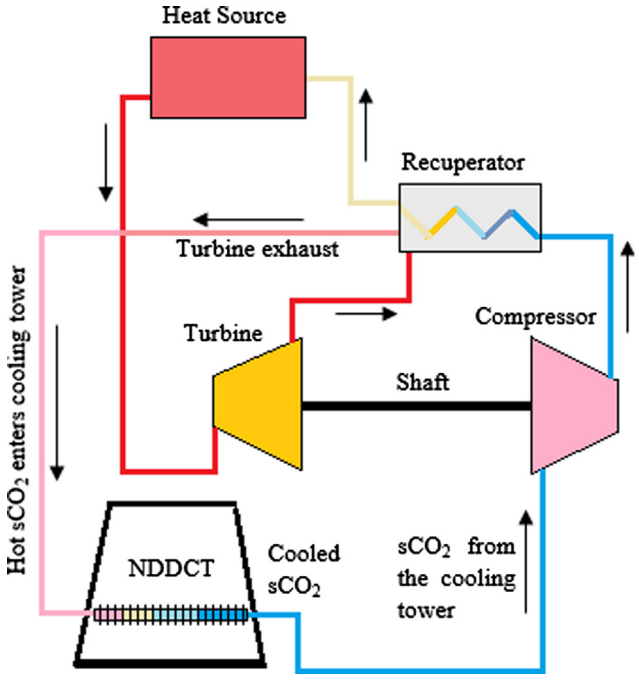

Fig. 1. Direct dry cooling system.

tube heat exchanger. The cooling water rises in temperature and is sent back to the air cooled heat exchanger unit inside a NDDCT where it is again cooled down. Certainly, an additional cost is associated with an extra component of shell and tube heat exchanger comparing with the direct cooling system.

3. Analysis of NDDCT

In a NDDCT, air travels through the bundles of finned tube heat exchanger unit by means of buoyant force due to the density difference between the warm air inside and the ambient air outside. Various loses are experienced by the air stream due to flow resistances while flowing in different parts of NDDCT. Table 1 shows the various loss coefficient equations in NDDCT which are used in the present analysis [26]. The driving force must overcome these flow resistances. By adding all these flow resistances, the draft equation is expressed by the following equation.

$$p_{a1}-\left[p_{a5}+\frac{\left(\frac{m_a}{A_5}\right)^2}{2\rho_{a5}}\right]=(K_{ts}+K_{ct}+K_{hes}+K_{ctc}+K_{he}+K_{cte})\frac{\left(\frac{m_a}{A_{fr}}\right)^2}{2\rho_{a34}}+p_{a1}\left[1-\left\{1-0.00975\frac{(H_3+H_4)}{2T_{a1}}\right\}^{3.5}\right]+p_{a4}\left[1-\left\{1-0.00975\left(H_5-\frac{H_3}{2}-\frac{H_4}{2}\right)T_{a4}\right\}^{3.5}\right] \quad (1)$$

4. Analysis of pre-cooler

For the analysis of pre-cooler, shell and tube exchanger is employed where water flows in the shell side and the high pressure sCO_2 flows in tube side. In the present work, counter flow-single pass shell and tube exchanger is employed and tubes are arranged with triangular layout pattern. A number of baffles are placed in the shell side to support the tubes with proper spacing and allow the shell side fluid to flow across the tubes in a specified manner. Fig. 3 shows the geometry of a segmental baffle used in the present work. The major constituents of a single pass shell and tube heat exchanger is shown in Fig. 4. Appendix A list all the equations used for the design of the shell and tube heat exchanger in the present analysis.

Table 2 shows the summery of all equations for the shell and tube heat exchanger which are used in the present analysis. The shell side heat transfer and pressure drop are the function of baffle spacing, length of baffle cut and various bypass and leakage flow. The correction factors for shell side heat transfer and pressure drop are shown in Table A1.

5. Analysis of air cooled heat exchanger

Air cooled heat exchanger unit is an essential element in NDDCT where the hot working fluid is cooled by the air stream flowing across the bundles of finned tube exchanger. The air side surface area is augmented by employing transversal circular fins on the bare tubes as shown in Fig. 5. Staggered arrangement of tubes provides better heat transfer performance in comparison with inlined arrangement. Appendix B lists all the equations used in the present analysis for the

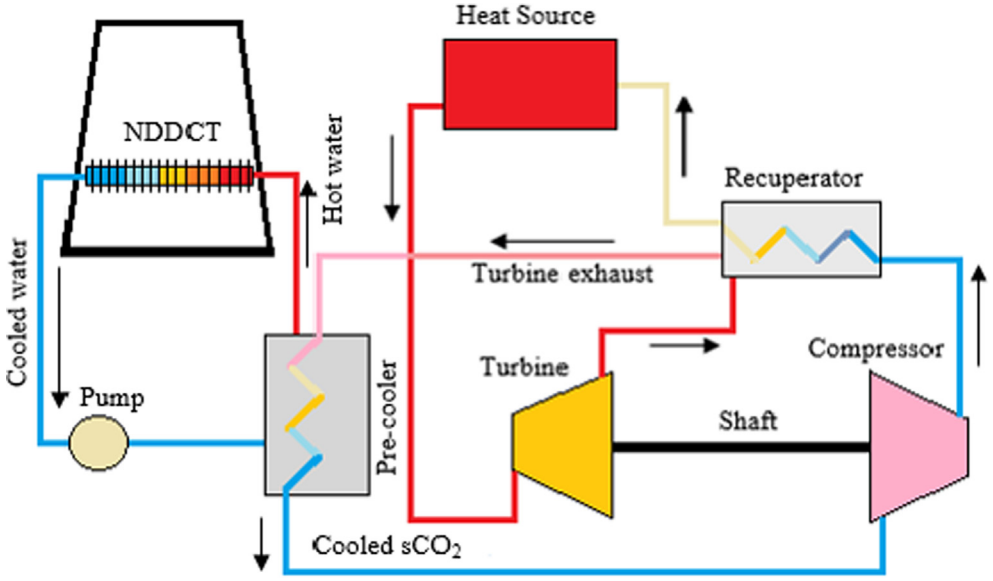

Fig. 2. Indirect dry cooling system.

Table 1
Loss coefficient equations for NDDCT [26].

Loss coefficient	Equation
The tower support loss efficient K_{ts}	$K_{ts} = \frac{2\Delta p_{ats}\rho_{a34}}{(\frac{m_a}{A_{fr}})^2} = \frac{C_{Dts}L_{ts}d_{ts}n_{ts}A_{fr}^2}{(\pi d_3 H_3)^3}(\frac{\rho_{a34}}{\rho_{a1}})$
Contraction loss efficient, K_{ctc}	$K_{ctc} = (1-\frac{2}{\sigma_c} + \frac{1}{\sigma_c^2})(\frac{\rho_{a34}}{\rho_{a1}})(\frac{A_{fr}}{A_{e3}})^2$
Expansion loss efficient, K_{cte}	$K_{cte} = (1-\frac{A_{e3}}{A_3})^2(\frac{\rho_{a34}}{\rho_{a1}})(\frac{A_{fr}}{A_{e3}})^2$
Cooling tower inlet loss coefficient, K_{ct}	$K_{ct} = K_{cthe}(\rho_{a34}/\rho_{a1})(A_{fr}/A_3)^2$ Terblanche and Kroger [27] correlation
	$K_{cthe} = [100-18(\frac{d_3}{H_3}) + 0.94(\frac{d_3}{H_3})^2]xK_{he}^{[-1.28+0.183(\frac{d_3}{H_3})-7.769x10^{-3}(\frac{d_3}{H_3})^2]}$
Cooling tower outlet loss coefficient K_{to}	$K_{to} = \frac{\Delta p_{a56}}{\frac{\rho_{a5}v_{a5}^2}{2}} = \frac{2\rho_{a5}\Delta p_{a56}}{(\frac{m_a}{A_5})^2} = -0.28Fr_D^{-1} + 0.04Fr_D^{-1.5}$
	$Fr_D = (\frac{m_a}{A_5})^2/[\rho_{a5}(\rho_{a6}-\rho_{a5})gd_5]s$
Heat exchanger loss coefficient, K_{he}	Characteristic Reynolds number, $Ry = \frac{m_a}{\mu_{a34}A_{frT}}$
	$K_{he} = 31383.9475Ry^{-0.332458} + \frac{2}{\sigma_a^2}(\frac{\rho_{a3}-\rho_{a4}}{\rho_{a3}+\rho_{a4}})$

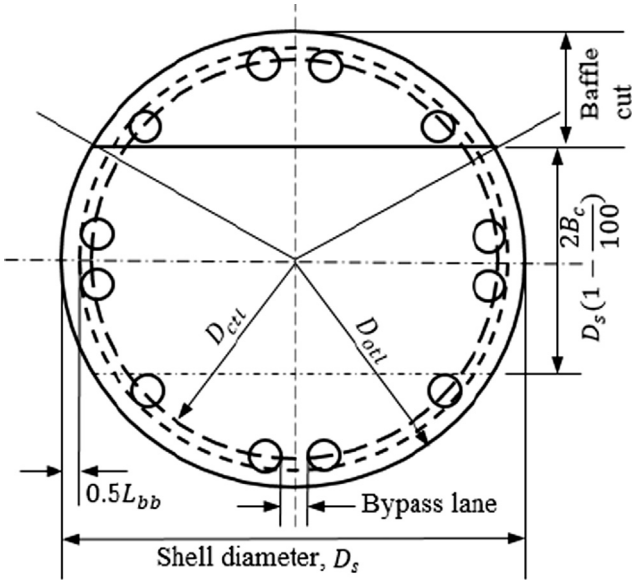

Fig. 3. Segmental baffle geometry.

design of air cooled heat exchanger unit.

6. Code validation

For the validation of the present code, Kroger's one dimensional model of heat exchanger [26] is used. Water is taken as working fluid in an air cooled heat exchanger which is modelled as four tube rows and one pass. In the Kroger model, all the thermodynamic and fluid dynamic parameters are evaluated by considering the overall geometry of the heat exchanger, whereas in the present code, nodal approach is adapted for the modelling of heat exchanger. In the nodal approach, a number of heat exchangers are assumed to be connected in series while the thermodynamic property (specific heat, density, viscosity and thermal conductivity) variation with bulk temperature and along the heat exchanger length are taken into consideration. Table 3 shows the code validation results comparing against Kroger model for two cases of water inlet temperature of 50 °C and 60 °C. For both cases, ambient air temperature is taken as 20 °C. The air side property variations along the length of the heat exchanger and across the tube rows are also taken into consideration. The result shows good agreement with the Kroger's model. Water is a constant property fluid and with the change of bulk temperature, the heat transfer coefficient of water remains almost constant. Therefore Kroger model is accurate to model the heat exchanger with constant property fluids. However, Kroger model fails to address nonlinear and the dramatic change of sCO_2 properties with bulk temperature. The nodal approach adapted in the present code justifies the sectioning of heat exchangers in order to capture the drastic sCO_2 property variation with the bulk temperature.

7. Model setup and preparation

In direct dry cooling system, air cooled heat exchanger unit is employed in the cooling tower to cool the hot sCO_2 by the ambient air flowing across the bundles of heat exchangers, shown in Fig. 6. The heat exchangers are horizontally arranged and tubes are in staggered configuration. The number of heat exchanger bundles is evaluated from the present code. The height of the tower for the required heat rejection determines the required number of heat exchanger bundles. The mass flow rate of sCO_2 is determined from the plant capacity.

On the other hand, for indirect cooling system, shell and tube heat exchanger is employed for the analysis of pre-cooler. The cooling water raises in temperature after absorbing heat from the sCO_2 in the pre-cooler. This water is cooled by the air cooled heat exchanger unit in NDDCT. For both cooling systems, same specification of air cooled heat exchanger unit is used. In order to model the NDDCT, the fixed geometric parameters are considered from the Kroger's [26] one dimensional model of cooling tower. The cooling tower is designed for an ambient air temperature of 15 °C, sCO_2 inlet temperature of 71 °C, operating sCO_2 pressure of 7.5 MPa and atmospheric pressure of 99,695 Pa for a 25 MW solar power plant. Table 4, shows the fixed geometric parameters for the design of NDDCT. Table 5, shows the specification of air cooled heat exchanger unit and shell and tube heat exchanger for the analysis of direct and indirect cooling system. The thermodynamic properties of sCO_2 are evaluated by linking the MATLAB with the software package REEFPROP 9.0 [31].

8. Mathematical model

8.1. Direct dry cooling system

The traditional method of modelling of heat exchanger are only valid for working fluid with constant properties. Nodal approach is adapted in designing the heat exchanger for sCO_2 cooling as shown in Fig. 7. In the nodal approach, each row of the heat exchanger bundles

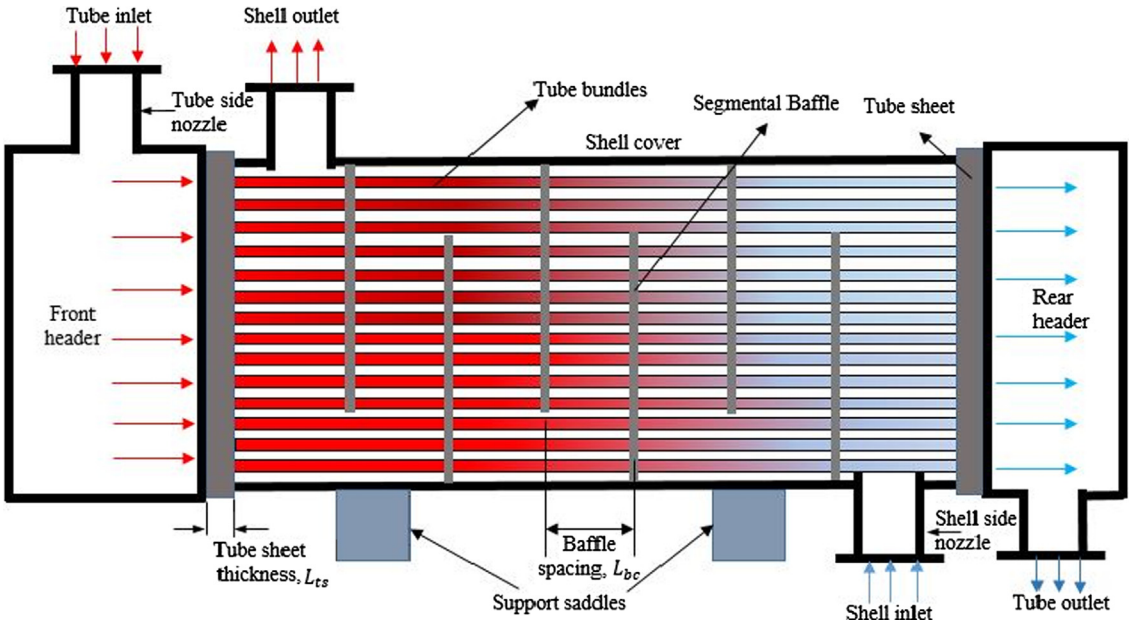

Fig. 4. Single pass counter flow shell and tube heat exchanger.

are divided into 30 sections, as if a number of small heat exchangers are connected in series. Therefore, the length of the finned tube for each section is 266 mm. The flow chart for the direct cooling system is shown in Fig. 8. The step by step procedures for designing the direct dry cooling system are described below.

i. All the fixed parameters of heat exchanger and specified geometric parameters of the cooling tower are given as inputs.
ii. With an initial assumption of cooling tower height, H_5, air mass flow rate, M_a, and air outlet temperature leaving the heat exchanger bundles, $T_{a4,}$ the code starts the calculation of pressure, temperature and density of air at different states of the cooling tower.
iii. Next, the code calculates all the loss coefficients K_{ts}, K_{ct}, K_{ctc}, K_{he}, K_{cte} and K_{to} experienced by the air stream at various states of tower.
iv. With all these calculated values, the code checks the draft equation. If the equation is not satisfied, the code adjusts the air mass flow rate. This required mass flow rate which satisfies the draft equation is used for the analysis of heat exchanger.
v. The dotted box represents the calculation of parameters for each section. For the first section in first row of tubes, both inlet temperature and pressure of sCO_2 and air are known. With an initial assumption of outlet temperatures, the energy equations for air-side, sCO_2 side and heat exchanger are simultaneously solved. The outlet temperatures which satisfy energy equation for each side are obtained for the calculation of next section.
vi. The outlet temperature and pressure for sCO_2 side are assigned as inputs for the calculation of the next section of the first row. The air inlet temperature and pressure are same at the inlet of first row of tubes.
vii. For the second row of tubes, air outlet temperatures and pressures are assigned as input air temperatures and pressures respectively. Similarly for third and fourth row of tubes, same procedure is applied.
viii. If the mean air outlet temperature leaving the heat exchanger bundles is not equal to the initial assumption of $T_{a4,}$ the code modifies the air outlet temperature. As a consequence, air mass flow rate, M_a is also changed. Hence, the steps v, vi, and vii are repeated.
ix. The total heat rejected by the tower is the sum of heat rejection by all 120 sections. Therefore, if the total heat rejection does not meet the desired heat rejection duty requirement, the code changes the cooling tower height, H_5.
x. Finally the output parameters are written in a specified file and the code finishes the calculation.

Table 6, shows the required parameters of NDDCT for direct dry cooling system. For single pass analysis, four different tube lengths (4 m, 6 m, 8 m and 10 m) of heat exchanger are considered in order to find an optimum size of tube length with minimum tower height and reasonable tube side pressure drop. Increasing the tube length, reduces the total surface area of air side and tube side for the same heat rejection. For all cases of single pass, desired outlet temperature of 40 °C is reached. The height of cooling tower also decreases with increased tube length. So for 4 m tube length, the tower requires a height of 48 m whereas for 10 m length tube, the tower requires a height of 44 m for the same heat rejection.

The 4 m tube length offers the lowest tube side pressure drop of 0.64 kPa due to lower mass flow rate and shorter tube length but it requires a higher tower height of 48 m. However, the 10 m tube length requires the lowest tower height of 44 m but the tube side pressure drop is significantly increased to 12.45 kPa due to higher mass flow rate and longer tube length. Although the 10 m tube length requires the lowest tower height, the optimum length of tube is chosen as 8 m with 45 m of tower height, since it offers better flexibility of arranging the heat exchanger bundles on the base of the tower. Also, the tube side pressure drop is within a reasonable limit for 8 m tube length. Therefore for indirect cooling system, 8 m tube length is chosen based on these factors. Multi-pass arrangement of tubes is also considered in the present analysis to investigate the influence of tube pass on the heat transfer mechanism. Double tube side pass with two different tube length of 6 m and 8 m is considered. In both cases, the sCO_2 outlet temperature is 45.9 °C and 46.18 °C respectively. Multi-pass arrangement of tubes is not appropriate for cooling of $sCO_{2,}$ since higher bulk temperature of sCO_2 is not desired at compressor inlet. Therefore multi-pass arrangement is not further considered for the analysis of indirect dry cooling system.

8.2. Indirect dry cooling system

Bell Delaware [32] method is employed in designing the shell and

Table 2
Summary of equations for shell and tube heat exchanger.

Parameter	Shell side	Tube side
Mass velocity	$G_s = \frac{M_s}{S_m}$	$G_t = \frac{N_p M_t}{A_t}$ $A_t = \frac{\pi}{4} d_i^2 N_t$
Reynolds number	$Re_s = \frac{d_o G_s}{\mu_s}$	$Re_t = \frac{d_i G_t}{\mu_t}$
Prandtl number	$Pr_s = \frac{\mu_s C_{ps}}{k_s}$	$Pr_t = \frac{\mu_t C_{pt}}{k_t}$
Energy equation	$Q = m_s c_{ps}(T_{so} - T_{si})$	$Q = m_t c_{pt}(T_{ti} - T_{to})$
Heat transfer correlation	$J_i = 1.73 Re_s^{-0.694}$ For $1 \leqslant Re_s < 100$ $J_i = 0.717 Re_s^{-0.574}$ For $100 \leqslant Re_s < 1000$, $J_i = 0.236 Re_s^{-0.346}$ For $1000 \leqslant Re_s$, The ideal heat transfer coefficient is given by, $h_i = \frac{J_i C_{ps} G_s (\varphi_s)^n}{Pr_s^{2/3}}$ Here $(\varphi_s)^n$ is the viscosity correction factor, $(\varphi_s)^n = (\frac{\mu_s}{\mu_w})^{0.14}$	Yoon et al. [29] correlation $Nu_t = a Re_t^b Pr_t^c (\frac{\rho_{pc}}{\rho_s})^n$ $a = 0.14$, $b = 0.69$, $c = 0.66$, $n = 0$ when $T > T_{pc}$ $a = 0.013$, $b = 1.0$, $c = -0.05$, $n = 1.6$ when $T \leqslant T_{pc}$
Friction factor	$f_s = \frac{52}{Re_s} + 0.17$ For $1 \leqslant Re_s < 500$ $f_s = 0.56 Re_s^{-0.14}$ For $500 \leqslant Re_s$	Churchill [30] correlation $f_t = 8\{(\frac{8}{Re_t})^{12} + [2.457 \ln(\frac{1}{(\frac{7}{Re_t})^{0.9} + 0.27\frac{\varepsilon}{d_i}})^{16} + (\frac{37530}{Re_t})^{16}]^{-1.5}\}^{\frac{1}{12}}$
Pressure drop	The total shell side pressure drop, $\Delta P_s = \Delta P_c + \Delta P_w + \Delta P_e$ The pressure drop for an ideal tube bank is given by, $\Delta P_b = 2 f_s N_{tcc} \frac{G_s^2}{g_c \rho_s} (\varphi_s)^{-n}$ The pressure drop in the interior cross section, $\Delta P_c = (N_b - 1)(\Delta P_b R_b R_l)$ The pressure drop for entrance and exit section is, $\Delta P_e = 2\Delta P_b (1 + \frac{N_{tcw}}{N_{tcc}}) R_b R_s$ The pressure drop for all the window section is, $\Delta P_w = \Delta P_{w,ideal} N_b R_l$ $\Delta P_{w,ideal} = \frac{(2 + 0.6 N_{tcw}) G_w^2}{2 g_c \rho_s}$ for $Re_s \geqslant 100$ $\Delta P_{w,ideal} = 26 \frac{G_w \mu_s}{g_c \rho_s} [\frac{N_{tcw}}{L_{tp} - d_o} + \frac{L_{bc}}{D_w^2}] + \frac{2 G_w^2}{g_c \rho_s}$ for $Re_s < 100$ The window mass velocity G_w is given by, $G_w = \frac{M_s}{\sqrt{S_m S_w}}$	The area-ratio for the tube side, $\sigma_s = \frac{A_{ts}}{P_t P_l}$ The contraction ratio is given by $\sigma_c = 0.61375 + 0.13318\sigma_s - 0.26095\sigma_s^2 + 0.51146\sigma_s^3$ Pressure drop in the nozzles, $\Delta P_n = \frac{1.5 G_t^2}{2 g_c \rho_t}$ Tube side contraction loss coefficient, $K_c = (1 - \frac{1}{\sigma_c})^2$ Tube side expansion loss coefficient, $K_e = (1 - \sigma_s)^2$ Pressure drop due to expansion and contraction losses, $\Delta P_{ce} = \frac{G_t^2}{2 g_c \rho_t} [K_c + K_e] N_p$ Pressure drop through the tube bundle, $\Delta P_b = \frac{f_t L_{ta} N_p G_t^2}{2 g_c \rho_t d_i}$ Pressure drop due to turning losses, $\Delta P_r = \frac{4 N_p G_t^2}{2 g_c \rho_t}$ Total tube side pressure drop, ΔP_t is expressed by, $\Delta P_t = \frac{N_p G_t^2}{2 g_c \rho_t} [\frac{1.5}{N_p} + \frac{f_t L_{ta}}{d_i} + K_c + K_e]$

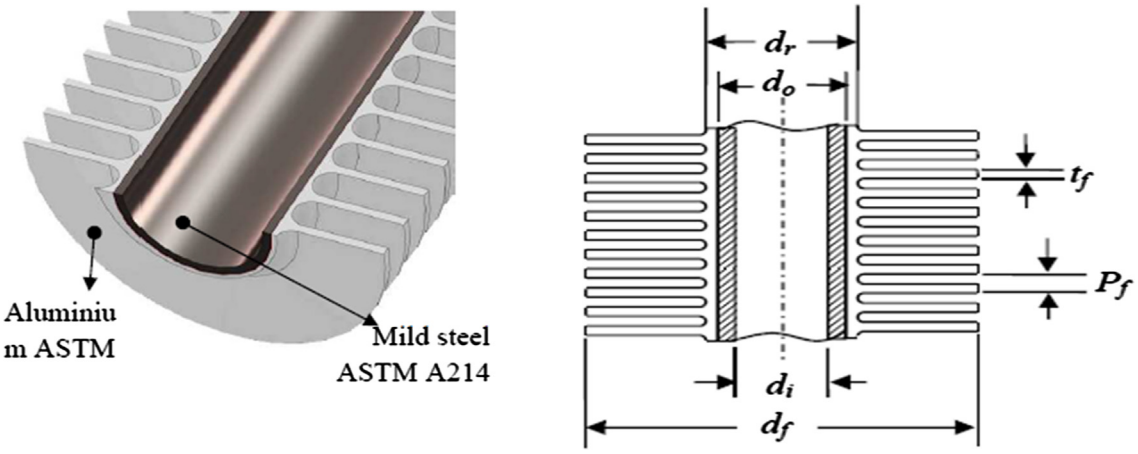

Fig. 5. Specification of different parameters for a transversal circular fin [28].

tube heat exchanger for the analysis of precooler. The flow chart for the analysis of pre-cooler is shown in Fig. 9. The nodal approach is again adapted to capture the sCO_2 thermodynamic property variations with the bulk temperature. In the optimized geometry, the heat exchanger contains 31 baffles. Therefore, for each baffle spacing, the property variations for both shell side and tube side are taken into consideration. The step by step procedure is described below.

i. All the fixed geometric parameters of heat exchanger are given as inputs. The code starts calculation with an initial assumption of baffle cut, B_c and baffle spacing L_{bc}.
ii. Next, the code calculates outer tube limit diameter $D_{otl,}$ centre line tube limit diameterD_{ctl}, shell length L_{to}, Number of baffles N_b, θ_{ds} and θ_{ctl}.
iii. The code assume a value of tube pitch, L_{tp} and calculates the total number of tubes, N_t.
iv. Next, the code calculates S_m, S_{wg}, F_w, F_c, S_{wt}, S_w, D_w, N_{tcc}, N_{tew}, S_b,F_{sbp}, S_{sb} and S_{tb}. In order to reduce the bypass flow, the code assumes a number of sealing strips, N_{ss} and calculates the value of $r_{s,}$ r_{lm}, $r_{ss,}$ N_c and x.
v. If the value of correction factor, J_c is not equal to 1, the modifies the baffle cut B_c.
vi. Next, the code checks the values of correction factors J_1 and R_1 due to baffle leakage effect. If the values exceed the desired limit, the code modifies the parameters L_{bc} and L_{tp}.
vii. Next, the code checks the limiting values of the correction factors J_b and R_b due to bundle bypass flow and modifies the parameter N_{ss} if necessary.
viii. With this optimized geometry of the heat exchanger, the code assumes values for water mass flow rate, M_s and water outlet temperature $T_{shell\_o.}$ In the nodal approach, each section of the heat exchanger has a length equal to the baffle spacing, $L_{bc.}$
ix. Next, the code calculates h_t, h_s, ΔT_{lm},ΔP_t, UA, Q_{hx}, Q_t and Q_s. The energy equations for shell side, tube side and heat exchanger are

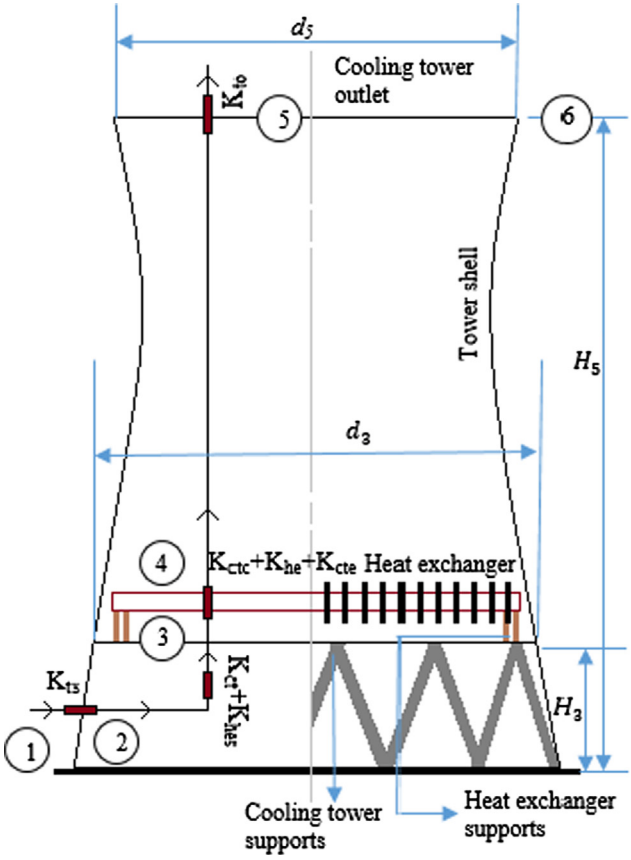

Fig. 6. Various air flow resistances in a NDDCT.

Table 3
Code validation against Kroger model.

Parameter	Water inlet temperature = 50 °C			Water inlet temperature = 60 °C		
	Kroger model	Present code	Mean Deviation	Kroger model	Present code	Mean Deviation
Water outlet temperature	47.3 °C	47.3 °C	< 1%	56.3 °C	56.3 °C	< 1%
Air outlet temperature	42.47 °C	42.46 °C	< 1%	50.04 °C	50.03 °C	< 1%
Total heat rejection	1.13 MW	1.13 MW	< 1%	1.51 MW	1.51 MW	< 1%
Average heat transfer coefficient of water	32,750 W/m^2 K	31,944 W/m^2 K	2.46%	37,055 W/m^2 K	36,142 W/m^2 K	2.45%
Average heat transfer coefficient of air	55.2 W/m ^{2}K	54 W/m^2 K	2.19%	55.5 W/m ^{2}K	54.3 W/m ^{2}K	2.12%
Water side pressure drop	52.2 kPa	52.2 kPa	< 1%	51.3 kPa	51.3 kPa	< 1%
Air side pressure drop	181 Pa	179 Pa	1.5%	186 Pa	184 Pa	1.25%

Table 4
Specified parameters for the design of 25 MW NDDCT.

Parameter	Value	Unit
Aspect ratio of cooling tower, H_5/d_3	1.4	–
Tower inlet height, H_3	10	m
Tower diameter ratio, d_5/d_3	0.7	–
Heat exchanger coverage of tower inlet, A_{frT}/A_3	0.7	–
Number of tower supports: n_{ts}	d_3/1.38	–
Length of tower support: *lts*	H_3 *x* 1.15	m
Drag coefficient of support, C_{Dts}	2	–
Diameter of tower support, d_{ts}	0.5	m

solved simultaneously. From the energy equation, the solution provides temperatures T_{tube_o} and T_{shell_i}.

x. For the calculation of next section, the outlet temperatures and pressures are assigned as inputs. For the remaining length of the heat exchanger, same procedure is applied.

xi. Next, the code checks the outlet temperature of sCO_2 at the end of tube and changes the water mass flow rate, M_s for the desired sCO_2 outlet temperature of 40 °C.

xii. Finally the code calls the function of NDDCT to check if the water temperature leaving the pre-cooler equals to the inlet water temperature of the cooling tower.

xiii. The air cooled heat exchanger cools the water inside NDDCT by adapting the nodal approach. The same procedure for direct cooling system is applied here and the code finishes the calculation.

9. Results and discussion

9.1. Single pass and multi-pass comparison

Fig. 10 shows the sCO_2 outlet temperatures, T_{so} at the end of each row of tubes for single pass and multi-pass arrangement in direct cooling system for sCO_2 inlet temperature of 71 °C and operating pressure of 7.5 MPa. Obviously, for multi-pass arrangement, the sCO_2 outlet temperatures at the outlet of heat exchanger are much higher

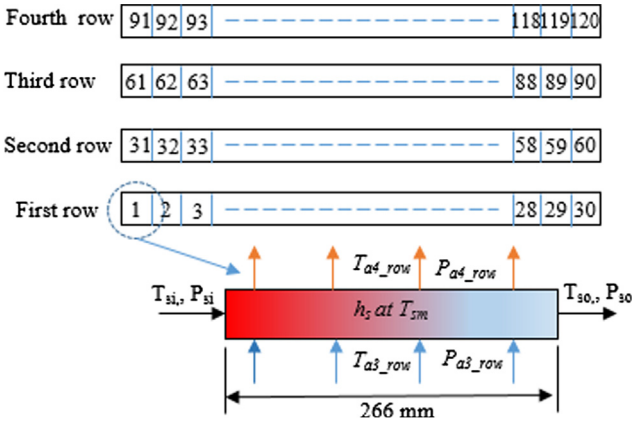

Fig. 7. Nodal approach for heat exchanger model.

(45.9 °C and 46.18 °C for tube length of 6 m and 8 m respectively) in comparison with single pass arrangement. Increasing the tube pass, certainly increase the mass flow rate. This higher mass flow rate in multi-pass tube arrangement, yields higher sCO_2 outlet temperature at the end of heat exchanger tubes. For all cases of single pass arrangement, sCO_2 outlet temperatures are almost same (40.1 °C, 40.4 °C, 40.3 °C and 40.5 °C for tube length of 4 m, 6 m, 8 m and 10 m respectively). In mutli-pass arrangement, the mass flow rate of sCO_2 in each tube is doubled, therefore the fluid gets less time to be cooled by the ambient air. Moreover, after sCO_2 passing through the first pass, the air side temperature increases. The initial temperature difference between the two fluid streams decreases for the second pass. That's why higher outlet temperature of sCO_2 is observed for multi-pass tube arrangement. The inlet process parameters are not same for multi-pass tube arrangement comparing with single pass cases, although the heat rejection duty is same for both cases.

Higher sCO_2 temperature indicates lower density which is not desired for compressor inlet condition and it requires higher compression work. Also for single pass arrangement of all cases, the sCO_2 outlet temperatures are much closer to the required design temperature of

Table 5
Specification of heat exchanger model.

Air cooled heat exchanger

Parameter	Value	Unit	Parameter	Value	Unit
Tube material	ASTM A214 mild steel	–	Fin type	Extruded bimetallic	–
Thermal conductivity of the tube, k_t	50	W/m K	Heat exchanger arrangement	horizontal	–
Tube outside diameter, d_o	25	mm	Fin Shape	Circular	–
Tube inside diameter, d_i	20	mm	Tube arrangement	staggered	–
Relative tube surface roughness, ε/d_i	5.24×10^{-4}	–	Fin material	ASTM 6063 aluminium	–
Number of tube rows, n_r	4	–	Thermal conductivity, k_f	204	W/mK
Effective no. of tubes per row, n_{tr}	47.5	–	Fin diameter, d_f	57	mm
No. of tubes per bundle, n_{tb}	190	–	Fin root diameter, d_r	28	mm
Transversal tube pitch, P_t	58	mm	Fin shape	Tapered	–
Longitudinal tube pitch, P_l	52	mm	Fin tip thickness, t_{ft}	0.25	mm
Length of the finned tube, L_t	8	m	Fin thickness (mean), t_f	0.5	mm
Width of the heat exchanger	2.47	m	Fin root thickness, t_{fr}	0.75	mm
Height of the heat exchanger	0.232	m	Fin Pitch, P_f	2.8	mm

Shell and tube heat Exchanger

Parameter	Value	Unit	Parameter	Value	Unit
Tube material	ASTM A214 mild steel	–	clearance between shell diameter and baffle diameter, L_{sb}	0.008	m
Bundle to shell clearance L_{bb},	0.0183	m	The centriangle of baffle cut, θ_{ds}	106.2	degree
Outer tube limit diameter, D_{otl}	1.23	m	The upper centriangle of baffle cut, θ_{ctl}	103.1	degree
Centreline tube limit diameter, D_{ctl}	1.20	m	The tube length, L_{ta}	10	m
The shell length, L_{to}	10.05	m	Tubesheet thickness, L_{ts}	0.025	m
Number of baffles, N_b	31	–	Tube layout pattern	Triangular	–
Number of tubes, N_t	939		Tube pitch ratio, L_{tp}/d_o	1.5	m

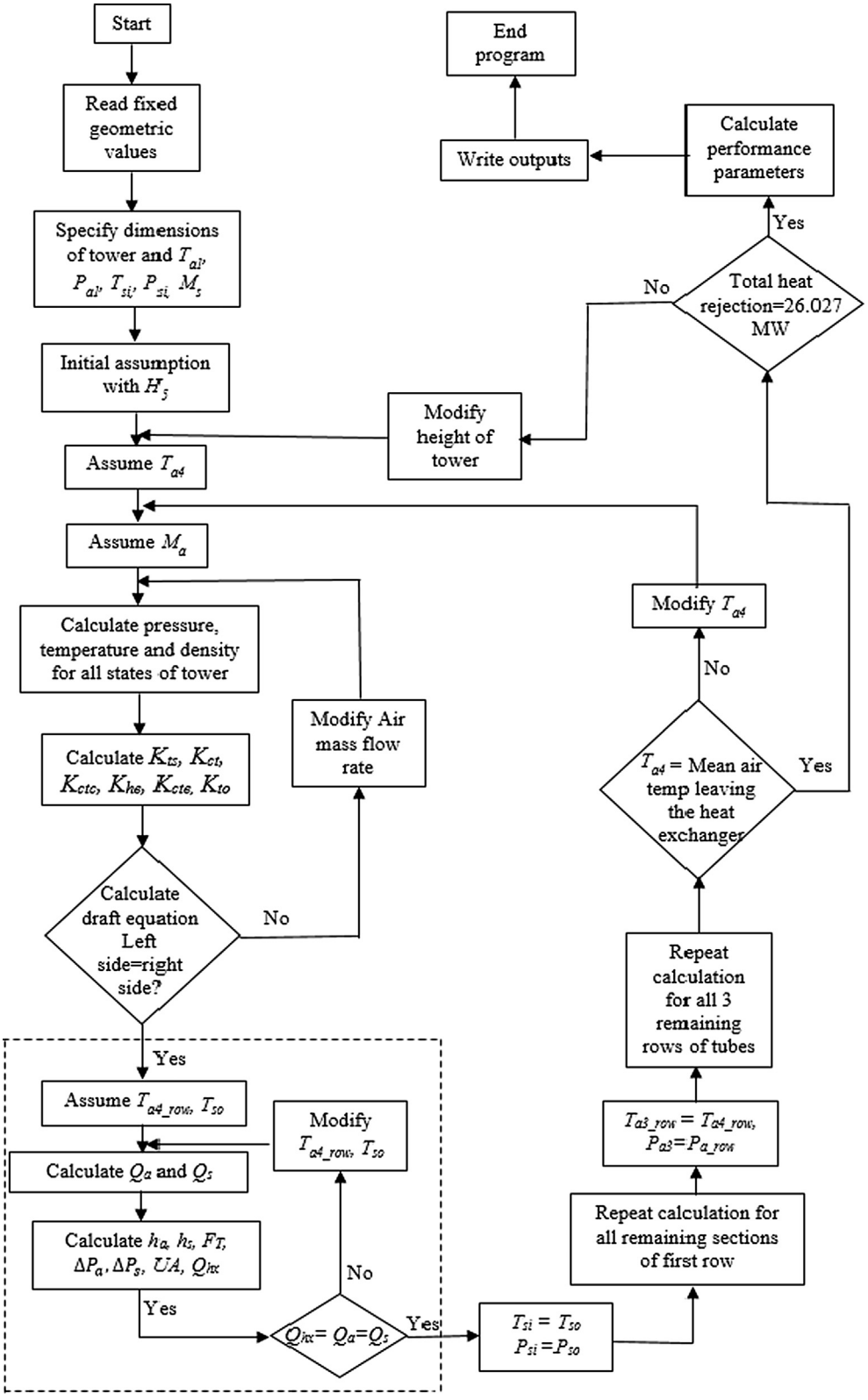

Fig. 8. Flow chart for direct dry cooling system.

40 °C. Therefore, the desired sCO_2 cooling performance is achievable in air cooled heat exchanger unit with single pass tube arrangement. Air outlet temperatures, T_{a4} at the end of each row of tubes are shown in Fig. 11, for single and multi-pass arrangement under the same operating condition. Air temperature gradually rises across the tube rows. For multi-pass arrangement, the outlet air temperatures are higher than single pass arrangement up to 3rd row position. For single pass arrangement, as the tube length increases from 4 m to 10 m, the air temperature at the outlet of heat exchanger bundles also increases from 40.9 °C to 45.1 °C.

The sCO_2 pressure drop variation, ΔP_s for single pass and multi-pass arrangement in direct cooling system is shown in Fig. 12. For tube

Table 6
Cooling system required for a 25 MW solar power plant.

Parameter	Direct cooling system					
	Single pass				Multi pass	
Number of pass, N_p	1	1	1	1	2	2
Outlet height of tower, H_5	48 m	46 m	45 m	44 m	47 m	46 *m*
Outlet tower diameter, d_5	24 m	23 m	22.5 m	22 m	23.5 m	23 m
Inlet tower diameter, d_3	34.2 m	32.8 m	32.1 m	31.4 m	33.5 m	32.8 m
Number of heat exchanger bundles, n_b	65	40	29	22	42	30
Number of tower supports: n_{ts}	25	24	24	23	24	24
Length of tower support: *lts*	11.5 m	11.5 m	11.5 m	11.4	11.5 m	11.5 m
Length of finned tube, L_t	4 m	6 m	8 m	10 m	6 m	8 m
Total air side surface area	72,672 m^2	67,082 m^2	64,846 m^2	61,492 m^2	70,437 m^2	67,082 m^2
Total tube side surface area	3104 m^2	2865 m^2	2769 m^2	2626 m^2	3008 m^2	2865 m^2
sCO_2 inlet temperature, T_{si}	71 °C	71 °C	71 °C	71 °C	71 °C	71 °C
sCO_2 mean outlet temperature, T_{so}	40.4 °C	40.4 °C	40.3 °C	40.5 °C	45.9 °C	46.18 °C
Air inlet temperature, T_{a3}	15 °C	15 °C	15 °C	15 °C	15 °C	15 °C
Air mean outlet temperature, T_{a4}	40.1 °C	42.8 °C	43.5 °C	44.5 °C	43.5 °C	44.7 °C
Tube side pressure drop, ΔP_s	0.64 kPa	2.63 kPa	5.83 kPa	12.45 kPa	6.4 kPa	15.1 kPa
Air side pressure drop, ΔP_a	118 Pa	119 Pa	123 Pa	127 Pa	117 Pa	121 Pa

length of 8 m, multi-pass arrangement requires the highest average pressure drop of 15.1 kPa due to larger tube length and higher mass flow rate. For single pass arrangement, as the tube length increases from 4 m to 10 m, the average pressure drop also increases significantly from 0.64 kPa to 12.45 kPa. Fig. 13**,** demonstrates the variation of local sCO_2 heat transfer coefficient, h_{sCO2} along the heat exchanger length of the first row of tubes for single and multi-pass arrangement. Since sCO_2 is cooled, the local heat transfer coefficient gradually increases along the tube length. For multi-pass arrangement, lower values of heat transfer coefficient are observed due to higher bulk temperatures in comparison with single pass arrangement. An increase in tube length, augments the sCO_2 mass flow rate. Therefore, for single pass arrangement, higher values of local heat transfer coefficient are achieved with finned tube length of 10 m. Similar trend of local heat transfer coefficient along the tube length is observed for 2nd, 3rd and 4th row of tubes in the heat exchanger bundles.

9.2. Direct dry cooling system

Fig. 14 shows the sCO_2 bulk temperature profile along the heat exchanger tube length for each tube rows. For the first row of tubes, sharp decrease of bulk temperature is observed, whereas for 2nd, 3rd, and 4th row, the slope is less steeper due to gradual increase of air temperature across each tube row. The sCO_2 temperature at the end of each row is also gradually increased (35.3 °C, 38.7 °C, 42.1 °C and 45.2 °C respectively).

Similarly, the variation of local heat transfer coefficient of sCO_2 along the tube length is shown in Fig. 15**.** For the first row of tubes, local heat transfer coefficient, h_{sCO2} increases dramatically due to the bulk temperature near critical point and higher temperature difference between two fluid streams. For the 2nd, 3rd and 4th row of tubes, the slope of local heat transfer coefficient is less steeper due to higher bulk temperature and gradual rise of air temperature across the tube rows.

The sCO_2 pressure drop characteristics are also investigated along the length of the tube of the heat exchanger bundles. At the inlet of tube, the pressure drop variation is more dominant due to higher Reynolds number and the bulk temperature. During cooling, the bulk temperature of sCO_2 decreases along the tube length, which causes the flow Reynolds number to be reduced due to higher density and viscosity. Higher values of pressure drop are observed for the remaining row of tubes in comparison with the first row (5.38 kPa, 5.74 kPa, 6.1 kPa and 6.21 kPa respectively). At any position along the tube length, the sCO_2 bulk temperature is higher as the row position is increased. This increased bulk temperature also augments the pressure drop across the tube row due to higher Reynolds number. The insignificant increase of sCO_2 pressure drop at the end of each row suggests the unique flow behaviour. However, in order to comply the flow characteristics of a parallel tube flow system, the unequal pressure drop of sCO_2 at the end of each row needs to be adjusted. In the present case, the unequal pressure drop of sCO_2 is addressed by the system by adjusting the mass flow rate. This ensures equal sCO_2 pressure drop for each tube row position as shown in Fig. 16.

The total heat rejection at the end of each row of the heat exchanger bundles is shown in Fig. 17**.** Since lower bulk temperature and higher local heat transfer coefficient are achieved in the first row of tubes, maximum heat rejection is obtained from the first row of tube. Heat rejected by sCO_2 decreases along the tube length due to gradual decrement of temperature difference between sCO_2 and ambient air. The total heat rejected by sCO_2 at the end of each row are 8.72 MW, 6.98 MW, 5.74 MW and 4.79 MW respectively.

9.3. Analysis of pre-cooler

Fig. 18**,** shows the sCO_2 bulk temperature profile and water temperature profile in the shell and tube heat exchanger. For each baffle spacing, both shell side and tube side temperatures are evaluated by the present code. Due to heat exchange in a single pass counter flow heat exchanger, sCO_2 is cooled to 40.3 °C whereas water temperature increases from 25.5 °C to 47.8 °C. Fig. 19**,** shows the variation of sCO_2 local heat transfer coefficient $h_{\_tube,}$ and local pressure drop ΔP_t along the heat exchanger tube length. $h_{\_tube}$ increases from 0.93 kW/m^2 K to 1.63 kW/m^2 K with the decrease of bulk temperature. The local heat transfer coefficient for shell side $h_{\_shell}$ varies from 3.58 kW/m^2 K to 2.97 kW/m^2 K. The higher bulk temperature of sCO_2 at the start of the tube increases the flow Reynolds number. Therefore, sCO_2 pressure drop decreases along the tube length. The total tube side pressure drop is 13.17 kPa.

Fig. 20**,** demonstrates the velocity profiles in the shell and tube heat exchanger. The tube side velocity *V_tube* gradually decreases along the tube length due to the decrease of flow Reynolds number and increase of viscosity and density. The variation in the tube side velocity (from 1.24 m/s to 0.86 m/s) is observed due to the change of transport properties of sCO_2 with the bulk temperature. Since, water properties do not show dramatic variation with the bulk temperature, the shell

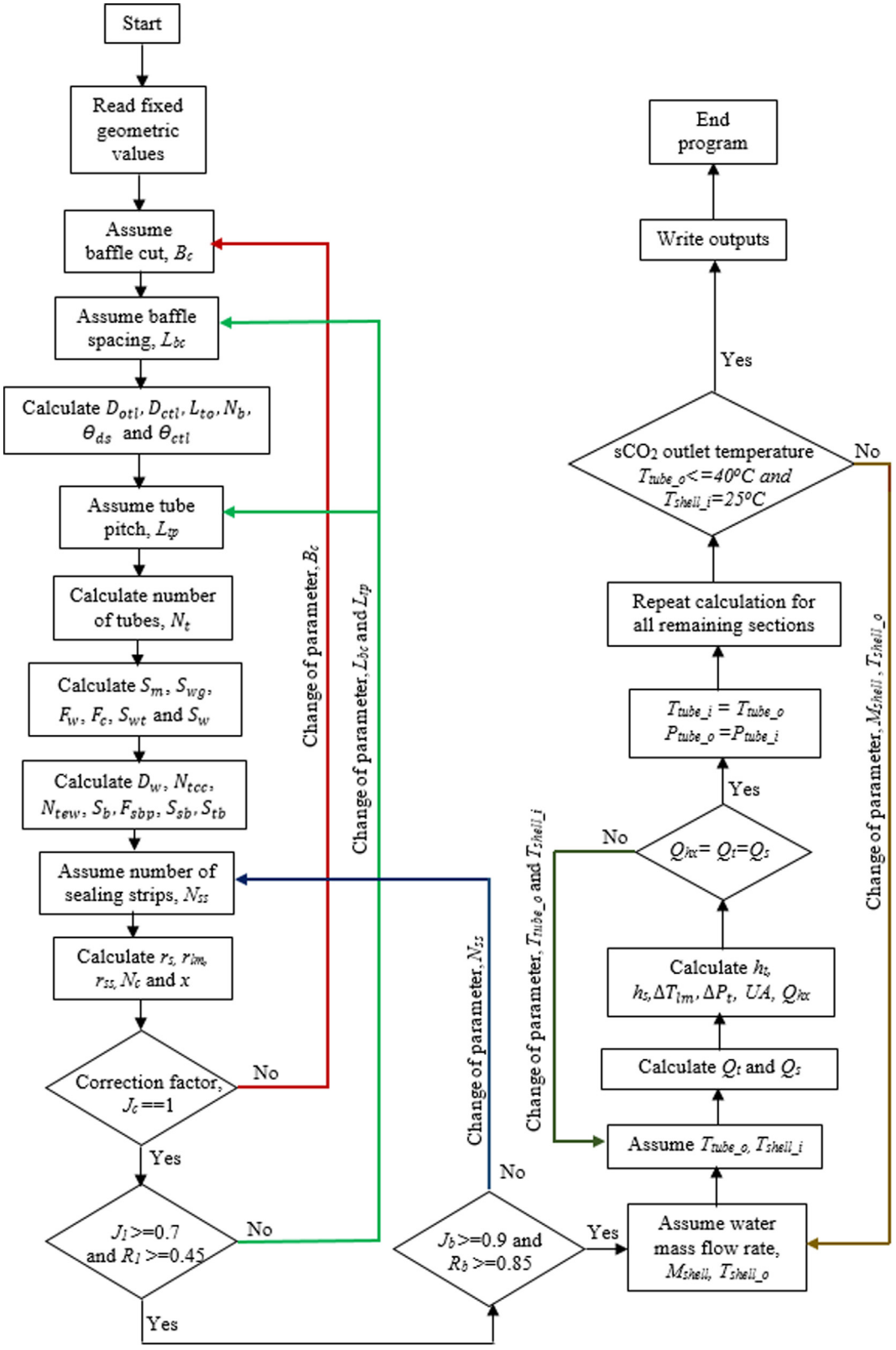

Fig. 9. Flow chart for the analysis of pre-cooler.

side velocity *V_shell* remains constant along the tube length. It is noted that each unit of shell and tube heat exchanger is able to reject 3.67 MW of heat. Therefore, 7 units of shell and tube heat exchangers arranged in parallel configuration are required for a 25 MW power plant.

9.4. Comparison of direct and indirect cooling system

Table 7 shows the required cooling system specification for direct and indirect cooling system. Obviously, an extra cost is associated of shell and tube heat exchanger unit in indirect cooling system.

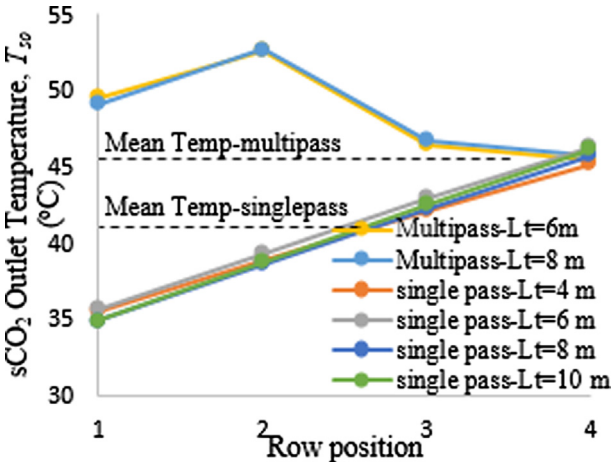

Fig. 10. sCO_2 outlet temperatures for single pass and multi-pass arrangement in direct cooling system.

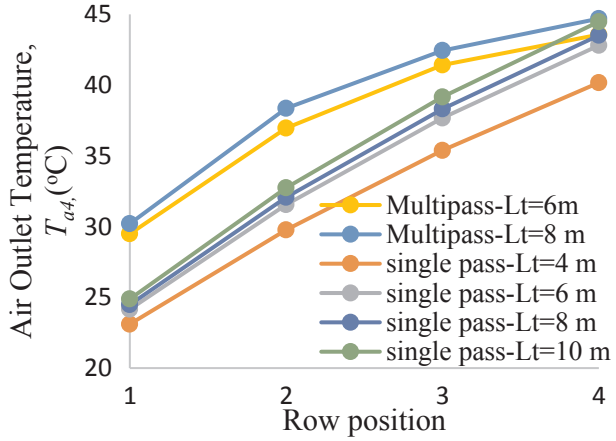

Fig. 11. Air temperatures for single pass and multi-pass arrangement in direct cooling system.

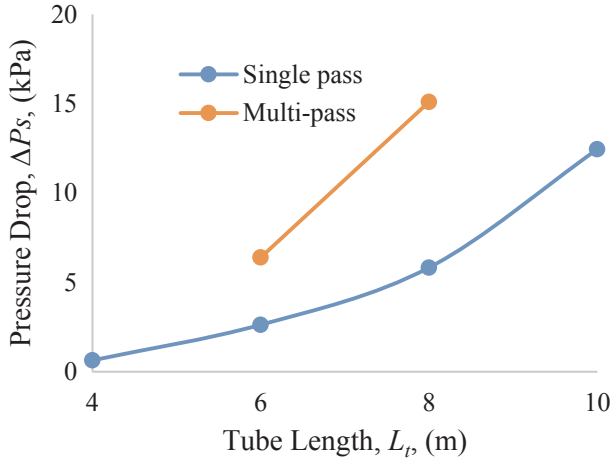

Fig. 12. sCO_2 pressure drop for single pass and multi-pass arrangement in direct cooling system.

Moreover, the required height of NDDCT for indirect cooling system is 63 m whereas for direct cooling system, the tower height is only 45 m for the same heat rejection duty. For direct cooling system, the higher initial temperature difference between sCO_2 and air requires the lower tower height. More bundles of air cooled hear exchangers are also required by the indirect cooling system (56 bundles for indirect comparing with 29 for direct cooling). The total surface area for air side and tube side significantly increases by 93% for indirect cooling system. Although from both cooling system, the desired sCO_2 mean outlet temperature of 40 °C is achieved but the capital cost for the indirect cooling system should be significantly higher in comparison with direct dry cooling system.

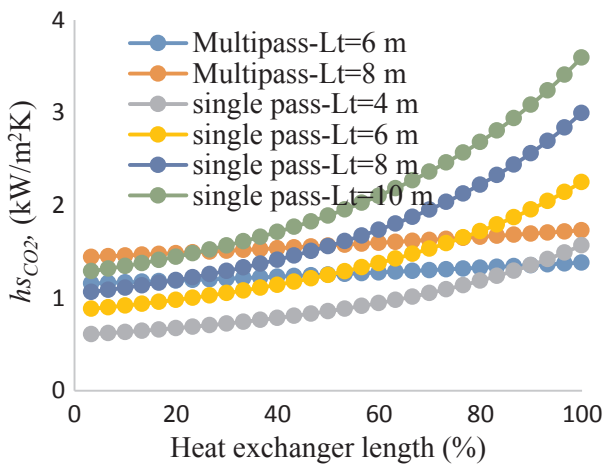

Fig. 13. Variation of local sCO_2 heat transfer coefficient for single pass and multi-pass arrangement.

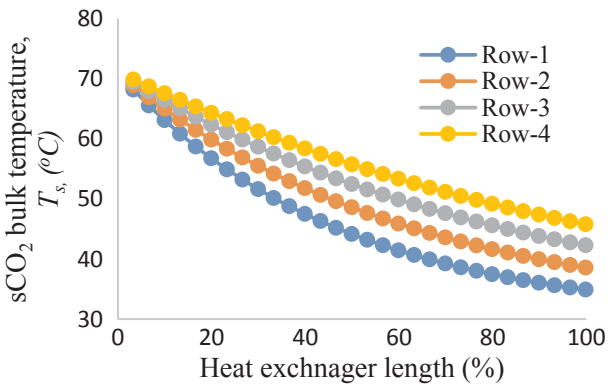

Fig. 14. sCO_2 bulk temperature variation along the heat exchanger length.

The change of air side properties is also taken into account by the present code. Fig. 21 shows the average air side heat transfer coefficient, h_a across each row of tubes for both cooling systems. The value of h_a slightly increases across the tube rows due to the minor change of air side thermodynamic properties. The average heat transfer coefficient of air is slightly higher for direct cooling system. The average air side

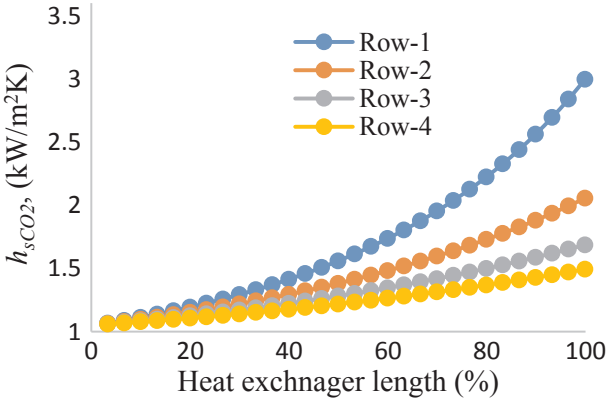

Fig. 15. sCO_2 local heat transfer coefficient along the heat exchanger length.

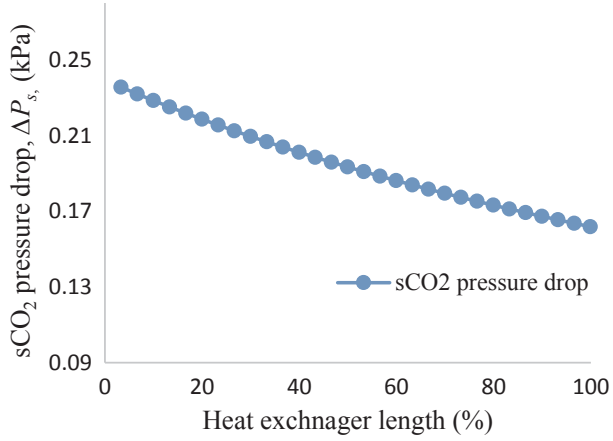

Fig. 16. sCO_2 pressure drop variation along the heat exchanger length.

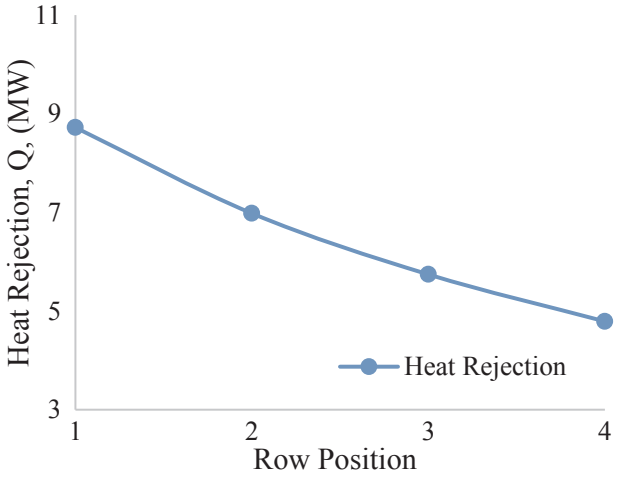

Fig. 17. Total heat rejection at the end of each row of heat exchanger.

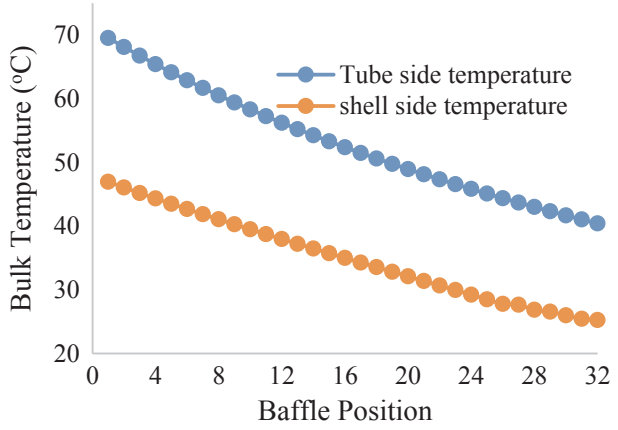

Fig. 18. Variation of bulk temperature in shell and tube heat exchanger.

pressure drop, ΔP_a is shown in Fig. 22. Since the value of h_a is higher for direct cooling system, an increase in ΔP_a is also observed compared to indirect system. The thermal conductivity of air, k_a increases with air temperature. This causes the air side pressure drop, ΔP_a to be increased insignificantly across each tube row position. The total air side pressure drop is 123 Pa and 114 Pa for direct and indirect cooling system respectively.

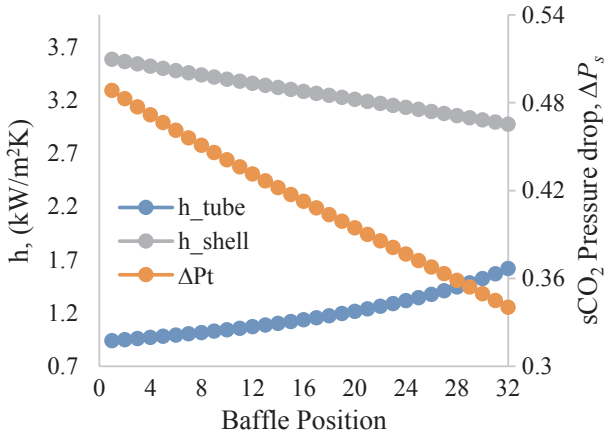

Fig. 19. Variation of local heat transfer coefficient and pressure drop along each baffle position.

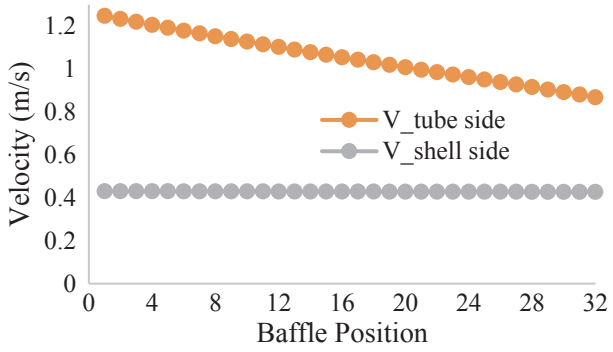

Fig. 20. Variation of shell side and tube side velocities along the heat exchanger length.

Table 7
Cooling system required for direct and indirect cooling systems.

Parameter	Direct dry cooling system	Indirect dry cooling system
Number of pass, N_p	1	1
Outlet height of tower, H_5	45 m	63 m
Outlet tower diameter, d_5	22.5 m	31.5 m
Inlet tower diameter, d_3	32.1 m	45 m
Number of heat exchanger bundles, n_b	29	56
Number of tower supports: n_{ts}	24	33
Length of tower support: *lts*	11.5 m	11.5 m
Length of finned tube, L_t	8 m	8 m
Total air side surface area	64,846 m^2	1,25,222 m^2
Total tube side surface area	2769 m^2	5348 m^2
sCO_2/water inlet temperature	71 °C	47.8 °C
sCO_2/water inlet pressure	7.5 MPa	0.1 MPa
sCO_2 mean outlet temperature	40.3 °C	40.3 °C
Air mean outlet temperature, T_{a4}	43.5 °C	29.8 °C

Fig. 23 reports the mean outlet temperatures in NDDCT for direct and indirect cooling system. The air outlet temperature increases sharply across each tube row for direct cooling system due to higher initial temperature difference between two fluid streams. However, for indirect cooling system, the air outlet temperature is much lower than direct system and increases insignificantly across each tube row. The outlet temperature of sCO_2 at the end of each row of tubes is higher than water outlet temperatures. The lower initial temperature difference between water and air in indirect cooling system certainly requires

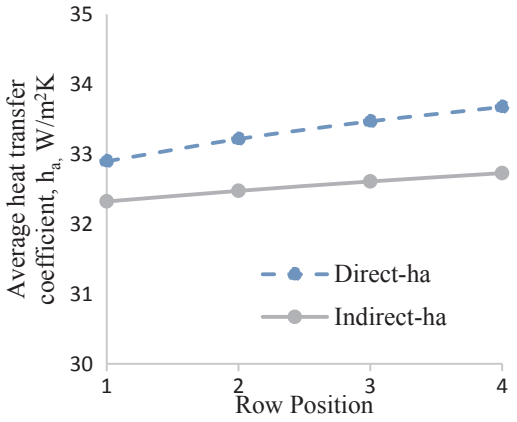

Fig. 21. Air-side heat transfer coefficient across each the tube rows.

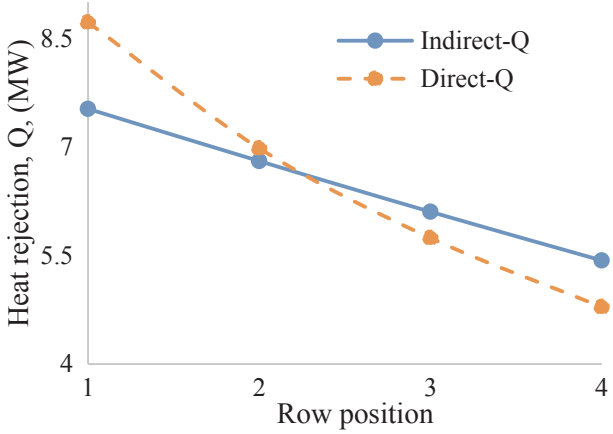

Fig. 24. Heat rejection profile for direct and indirect cooling system.

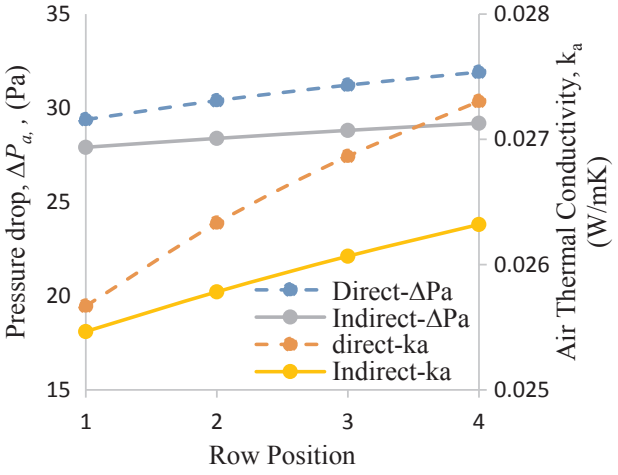

Fig. 22. Variation of air-side pressure drop and thermal conductivity across the tube rows.

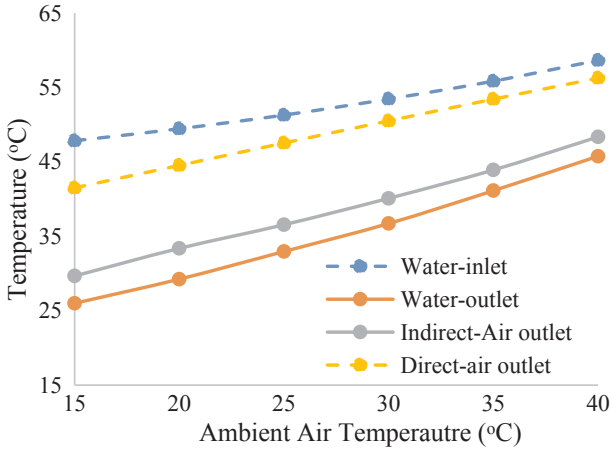

Fig. 25. Outlet temperatures at various ambient temperature for indirect cooling system.

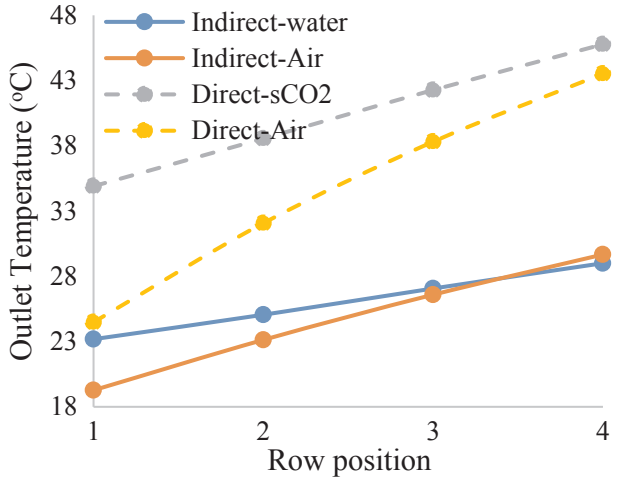

Fig. 23. Mean outlet temperatures for direct and indirect cooling system.

higher tower height to dissipate the same amount of heat. Fig. 24 shows the heat rejection profile in air cooled heat exchanger for both cooling systems. As the temperature difference between the working fluid and air decreases across the tube row, highest amount of heat is rejected by the first row of tubes. The heat rejection profiles are almost identical for both direct and indirect cooling system.

The influence of different ambient temperature on the performance of NDDCT for both cooling systems is performed in the present article. Fig. 25 shows the water inlet, water outlet and air outlet temperatures at various ambient temperature for indirect cooling system. Certainly, raising the ambient temperature from 15 °C to 40 °C increases the water inlet temperatures in the NDDCT. This higher water temperature increases the sCO_2 outlet temperature in the pre-cooler. At higher ambient temperature period, the sCO_2 outlet temperature is higher for indirect cooling system. Therefore, during high ambient temperature period, direct cooling system shows better cooling performance in comparison with indirect cooling system.

Fig. 26 shows the heat rejection profiles for both direct and indirect cooling system under various ambient temperature. Increasing the ambient temperature increases the mean sCO_2 outlet temperature in the heat exchanger. Therefore, the total heat rejection, Q decreases during high ambient temperature period. For indirect cooling system, during high ambient temperature period, water inlet temperature in NDDCT increases which also increases the sCO_2 outlet temperature in the shell and tube heat exchanger. Since with direct cooling system, lower sCO_2 outlet temperature is achieved at any ambient temperature, higher amount of heat is rejected in comparison with indirect cooling system.

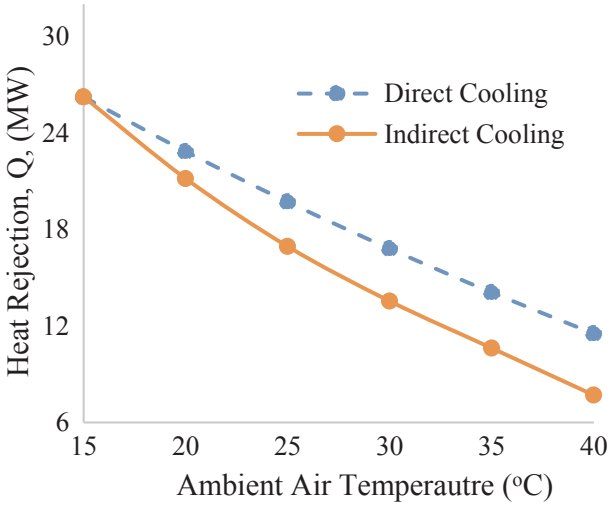

Fig. 26. Influence of ambient temperature on heat rejection for direct and indirect cooling system.

10. Conclusion

- In present article, cooling system is designed and compared for a 25 MW solar power plant. The validated present code is fully capable in predicting the heat transfer mechanism and fluid flow behaviour in the heat exchangers. The rapid property variation of sCO_2 is well captured by the iterative nodal approach.
- In the present code, the changes of properties for both airside and sCO_2 side are taken into consideration. The change of local heat transfer coefficient of sCO_2 with the bulk temperature as well as along the length of tubes is reasonably well predicted by the present code. The code is also able to address the change of air side properties along the heat exchanger length and across the tube rows
- The required size of the NDDCT for direct and indirect cooling system is proposed. Due to higher initial temperature between two fluid streams, direct cooling system requires smaller tower height in comparison indirect cooling system.
- Single pass and multi-pass arrangement of tubes are considered in order to explore the effect of tube pass on the heat transfer mechanism and pressure drop characteristics. Multi-pass arrangement of tubes is not favourable for sCO_2 cooling since, higher sCO_2 outlet temperature is not desirable for compressor inlet.
- For the analysis of pre-cooler, an optimum size of shell and tube heat exchanger is selected in order to keep the shell side heat transfer and pressure drop correction factors within a reasonable limit.
- For indirect cooling system, a higher tower height is required due to lower initial temperature difference between water and air in NDDCT. Moreover, at higher ambient temperature, the water inlet temperature in the tower increases which adversely affect heat transfer mechanism in the pre-cooler.
- During high ambient temperature period, dry cooling system provides better cooling performance in comparison with indirect cooling system in terms of lower sCO_2 outlet temperature.

Acknowledgement

This research was conducted as a part of the Australia Solar Thermal Research Initiative (ASTRI), a project supported by Australia government through the Australia Renewable Energy Agency (ARENA). The first author, M. Monjurul Ehsan would also like to acknowledge University of Queensland (UQ) for providing Research Training Program (RTP) and Australian Postgraduate Award (APA) scholarships.

Appendix A

For a fixed tube sheet heat exchanger, bundle to shell clearance L_{bb}, is given by

$$L_{bb} = 12 + 0.005D_s\,(\text{mm}) \tag{A.1}$$

Outer tube limit diameter,

$$D_{otl} = D_s - L_{bb} = D_{ctl} + d_o \tag{A.2}$$

The centreline tube limit diameter,

$$D_{ctl} = D_{otl} - d_o \tag{A.3}$$

The shell length,

$$L_{to} = L_{ta} + 2L_{ts} \tag{A.4}$$

The number of baffles,

$$N_b = \frac{L_{ta}}{L_{bc}} - 1 \tag{A.5}$$

The centriangle of baffle cut,

$$\theta_{ds} = 2\cos^{-1}\left(1 - \frac{2B_c}{100}\right) \tag{A.6}$$

The upper centriangle of baffle cut,

$$\theta_{ctl} = 2\cos^{-1}\left[\frac{D_s}{D_{ctl}}\left(1 - \frac{2B_c}{100}\right)\right] \tag{A.7}$$

The total number of tubes,

$$N_t = \frac{0.78D_{ctl}^2}{C_1 L_{tp}^2} \tag{A.8}$$

C_1 is 0.86 for triangular tube layout pattern

Shell side cross flow area,

Table A1
List of correction factors for shell and tube heat exchanger.

Shell side heat transfer correction factor	Parameter	Equation	Remarks
	J_c	$J_c = 0.55 + 0.72F_c$	Due to baffle cut and spacing
	J_1	$J_1 = 0.44(1-r_s) + [1-0.44(1-r_s)]ve^{-2.2r_{lm}}$ $r_s = \frac{S_{sb}}{S_{sb}+S_{tb}}$ $r_{lm} = \frac{S_{sb}+S_{tb}}{S_m}$	Due to shell to baffle leakage and tube to baffle leakage
	J_b	$J_b = \exp\{-C_{bh}F_{sbp}[1-(2r_{ss})^{\frac{1}{3}}]\}$ for $r_{ss} < 0.5$ $J_b = 1$ for $r_{ss} \geqslant 0.5$ $r_{ss} = \frac{N_{ss}}{N_{tcc}}$ C_{bh} is 1.25 for laminar flow ($Re_s < 100$) and 1.35 for turbulent and transition flow with $Re_s > 100$	Due to bundle bypass flow
	J_r	$J_r = \frac{1.51}{N_c^{0.18}}$ for $Re_s < 20$ $N_c = (N_{tcc} + N_{tcw})(N_b + 1)$ For $20 < Re_s < 100$ $J_r = \frac{1.51}{N_c^{0.18}} + (\frac{20-Re_s}{80})(\frac{1.51}{N_c^{0.18}}-1)$ The value of J_r is 1 for $Re_s > 100$	Due to adverse temperature gradient applicable for laminar flow
	J_s	$J_s = \frac{(N_b-1)+(\frac{L_{bi}}{L_{bc}})^{1-n}+(\frac{L_{b0}}{L_{bc}})^{1-n}}{(N_b-1)+(\frac{L_{bi}}{L_{bc}}-1)+(\frac{L_{bo}}{L_{bc}}-1)}$ For turbulent flow, the value of n is 0.6 and for laminar flow $Re_s < 100$, the value n is 0.33.	Due to variable baffle spacing in the inlet and outlet sections
	J	$J = J_cJ_1J_bJ_sJ_r$	Overall correction factor
Shell side pressure drop correction factor	R_1	$R_1 = \exp[-1.33(1 + r_s)]r_{lm}^x$ $x = [-0.15(1 + r_s) + 0.8]$	Due to baffle leakage effects
	R_b	$R_b = \exp\{-C_{bp}F_{sbp}[1-(2r_{ss})^{\frac{1}{3}}]\}$ for $r_{ss} < 0.5$ $R_b = 1$ for $r_{ss} \geqslant 0.5$ C_{bp} value is 4.5 for laminar flow ($Re_s < 100$) and 3.7 for turbulent and transition flow with $Re_s > 100$	Due to bundle bypass effects
	R_s	$R_s = (\frac{L_{bc}}{L_{bi}})^{2-n} + (\frac{L_{bc}}{L_{bo}})^{2-n}$ For turbulent flow, the value of n is 0.2 and for laminar flow $Re_s < 100$, the value n is 1	Due to unequal baffle spacing

$$S_m = L_{bc}\left[L_{bb} + \frac{D_{ctl}}{L_{tp}}(L_{tp}-d_o)\right] \tag{A.9}$$

The gross window flow area,

$$S_{wg} = \frac{\pi}{4}D_s^2\left(\frac{\theta_{ds}}{2\pi} - \frac{sin\theta_{ds}}{2\pi}\right) \tag{A.10}$$

The total number of tubes is the sum of the fraction of tubes in baffle window, F_w and in pure cross flow, F_c.

$$F_c = 1-2F_w \tag{A.11}$$

The fraction of the tubes in the baffle window,

$$F_w = \frac{\theta_{ctl}}{2\pi} - \frac{sin\theta_{ctl}}{2\pi} \tag{A.12}$$

The baffle window area occupied by the tubes,

$$S_{wt} = N_tF_w\frac{\pi}{4}d_o^2 \tag{A.13}$$

The net cross flow area through the baffle,

$$S_w = S_{wg}-S_{wt} \tag{A.14}$$

The hydraulic diameter of a segmental baffle,

$$D_w = \frac{4S_w}{\pi d_oN_tF_w + \pi D_s\theta_{ds}/2\pi} \tag{A.15}$$

The number of effective tube rows in pure cross flow,

$$N_{tcc} = \frac{D_s}{0.866L_{tp}}(1-\frac{2B_c}{100}) \tag{A.16}$$

The number of effective tube rows in the baffle window,

$$N_{tew} = \frac{0.8}{0.866 L_{tp}}\left[\frac{D_s B_c}{100} - \frac{D_s - D_{ctl}}{2}\right] \tag{A.17}$$

The bypass area between the shell and tube bundle,

$$S_b = L_{bc}(D_s - D_{otl} + d_o) \tag{A.18}$$

Bundle to shell bypass area fraction,

$$F_{sbp} = \frac{S_b}{S_m} \tag{A.19}$$

The diametral clearance between the shell diameter and baffle diameter is given by

$$L_{sb} = 3.1 + 0.004 D_s (\text{mm}) \tag{A.20}$$

The shell to baffle leakage area,

$$S_{sb} = \pi D_s \frac{L_{sb}}{2}\left[\frac{2\pi - \theta_{ds}}{2\pi}\right] \tag{A.21}$$

The tube to bundle hole leakage area,

$$S_{tb} = \frac{\pi}{4}[(d_o + 0.8 * 0.001)^2 - d_o^2] N_t (1 - F_w) \tag{A.22}$$

Product of overall heat transfer coefficient and area for shell and tube heat exchanger,

$$UA = \left[\frac{1}{h_t A_t} + \frac{1}{2\pi k_t N_t x L_{ta}} ln\frac{d_o}{d_i} + \frac{1}{h_s A_s}\right]^{-1} \tag{A.23}$$

Appendix B

Let us consider a small control volume located between the centrelines of two adjacent tubes and two adjacent fins in the upstream tube row. The minimum free flow area through this control volume is given by,

$$A_{cvc} = (P_t - d_r)(P_f - t_f) \tag{B.1}$$

The frontal area,

$$A_{cvfr} = P_t P_f \tag{B.2}$$

The total fin surface area for a control volume,

$$A_{cva} = 2\left[P_t P_l - \frac{\pi}{4} d_o^2\right] + \pi d_r (P_f - t_f) \tag{B.3}$$

The air porosity,

$$\sigma_a = \frac{A_{cvc}}{A_{cvfr}} \tag{B.4}$$

The air-side equivalent hydraulic diameter,

$$d_{ea} = \frac{4 A_{cvc} P_l}{A_{cva}} \tag{B.5}$$

The air mass velocity,

$$G_a = \frac{M_a}{(A_{frT} \sigma_a)} \tag{B.6}$$

The total effective air-side fin surface area,

$$A_f = n_r n_{tr} \frac{L_t}{P_f}\left[\pi\left\{\frac{2}{4}(d_f^2 - d_r^2) + d_f t_{ft}\right\}\right] \tag{B.7}$$

The exposed root area,

$$A_r = \pi n_r n_{tr} L_t d_r (P_f - t_f)/P_f \tag{B.8}$$

So the total air side surface area,

$$A_a = n_b (A_f + A_r) \tag{B.9}$$

The friction factor f_a is calculated from Robinson and Briggs [33] correlation and finally the static pressure drop across the tube row core is given by,

$$\Delta P_a = \frac{G_a^2}{2\rho_{ai}}\left[(1 - \sigma_a^2) + 2\left(\frac{\rho_{ai}}{\rho_{ao}} - 1\right) + f_a n_r \frac{A_a \rho_{ai}}{A_{cvc} \rho_{am}} - (1 - \sigma_a^2)\frac{\rho_{ai}}{\rho_{ao}}\right] \tag{B.10}$$

$$f_{RB} = 9.465 Re_a^{0.316}\left(\frac{P_t}{d_o}\right)^{-0.927}\left(\frac{P_t}{P_d}\right)^{0.515} \text{and} f_a = \frac{1}{2}\frac{d_{ea}}{P_l} f_{RB} \tag{B.11}$$

Air side convective heat transfer coefficient is determined from Briggs and Young [34] correlation.

$$\frac{h_a d_r}{k_{a34}} = 0.134 Pr_{a34}^{0.33} Re_a^{0.681}\left[\frac{2(P_f - t_f)}{d_f - d_r}\right]^{0.2}\left(\frac{P_f - t_f}{t_f}\right)^{0.1134} \tag{B.12}$$

The tube side heat transfer coefficient for sCO_2 is calculated from Yoon et al. [29] correlation and sCO_2 friction factor is evaluated from Churchill [30] correlation. The product of overall heat transfer coefficient and area for finned tube heat exchanger.

$$UA = \left[\frac{1}{(h_{sCO2} A_{sCO2})} + \frac{1}{2\pi k_t n_b n_{tb} L_t} ln\frac{d_o}{d_i} + \frac{1}{2\pi k_f n_b n_{tb} L_t} ln\frac{d_f}{d_o} + \frac{1}{(h_a e_f A_a)}\right]^{-1} \tag{B.13}$$

References

[1] Dostal V, Driscoll MJ, Hejzlar P, Todreas NE. A supercritical CO_2 gas turbine power cycle for next-generation nuclear reactors. Proc ICONE 2002;10:2002.
[2] Feher EG. The supercritical thermodynamic power cycle. Energy Convers 1968;8(2):85–90.
[3] Besarati SM, Goswami DY. Analysis of advanced supercritical carbon dioxide power cycles with a bottoming cycle for concentrating solar power applications. J Sol Energy Eng 2014;136(1):010904.
[4] Conboy T, Wright S, Pasch J, Fleming D, Rochau G, Fuller R. Performance characteristics of an operating supercritical CO_2 Brayton cycle. J Eng Gas Turbines Power 2012;134(11):111703.
[5] Al-Sulaiman FA, Atif M. Performance comparison of different supercritical carbon dioxide Brayton cycles integrated with a solar power tower. Energy 2015;82:61–71.
[6] Dyreby J, Klein S, Nellis G, Reindl D. Design considerations for supercritical carbon dioxide Brayton cycles with recompression. J Eng Gas Turbines Power 2014;136(10):101701.
[7] Conboy T, Carlson M, Rochau G. Dry-cooled supercritical CO_2 power for advanced nuclear reactors. J Eng Gas Turbines Power 2015;137(1):012901.
[8] Wang K, He Y-L. Thermodynamic analysis and optimization of a molten salt solar power tower integrated with a recompression supercritical CO_2 Brayton cycle based on integrated modeling. Energy Convers Manage 2017;135:336–50.
[9] Zhang Y, et al. Low-grade heat utilization by supercritical carbon dioxide Rankine cycle: analysis on the performance of gas heater subjected to heat flux and convective boundary conditions. Energy Convers Manage 2018;162:39–54.
[10] Milani D, Luu MT, McNaughton R, Abbas A. Optimizing an advanced hybrid of solar-assisted supercritical CO_2 Brayton cycle: a vital transition for low-carbon power generation industry. Energy Convers Manage 2017;148:1317–31.
[11] Song J, Li X-S, Ren X-D, Gu C-W. Performance improvement of a preheating supercritical CO_2 (S-CO_2) cycle based system for engine waste heat recovery. Energy Convers Manage 2018;161:225–33.
[12] Padilla RV, Too YCS, Benito R, Stein W. Exergetic analysis of supercritical CO_2 Brayton cycles integrated with solar central receivers. Appl Energy 2015;148:348–65.
[13] Li X, Duniam S, Gurgenci H, Guan Z, Veeraragavan A. Full scale experimental study of a small natural draft dry cooling tower for concentrating solar thermal power plant. Appl Energy 2017;193:15–27.
[14] Wang W, Zhang H, Liu P, Li Z, Lv J, Ni W. The cooling performance of a natural draft dry cooling tower under crosswind and an enclosure approach to cooling efficiency enhancement. Appl Energy 2017;186:336–46.
[15] Li X, Xia L, Gurgenci H, Guan Z. Performance enhancement for the natural draft dry cooling tower under crosswind condition by optimizing the water distribution. Int J Heat Mass Transf 2017;107:271–80.
[16] Li X, Gurgenci H, Guan Z, Wang X, Duniam S. Measurements of crosswind influence on a natural draft dry cooling tower for a solar thermal power plant. Appl Energy 2017;206:1169–83.
[17] Wang W, Lv J, Zhang H, Liu Q, Yue G, Ni W. A quantitative approach identifies the critical flow characteristics in a natural draft dry cooling tower. Appl Therm Eng 2018;131:522–30.
[18] Wang W, Lyu J, Zhang H, Liu Q, Yue G, Ni W. A performance enhancement of a natural draft dry cooling tower in crosswind via inlet flow field reconstruction. Energy Build 2018;164:121–30.
[19] Wang X, Yang L, Du X, Yang Y. Performance improvement of natural draft dry cooling system by water flow distribution under crosswinds. Int J Heat Mass Transf 2017;108:1924–40.
[20] Alavi SR, Rahmati M. Experimental investigation on thermal performance of natural draft wet cooling towers employing an innovative wind-creator setup. Energy Convers Manage 2016;122:504–14.
[21] Sadafi M, et al. An investigation on spray cooling using saline water with experimental verification. Energy Convers Manage 2016;108:336–47.
[22] Sun Y, Guan Z, Gurgenci H, Hooman K, Li X, Xia L. Investigation on the influence of injection direction on the spray cooling performance in natural draft dry cooling tower. Int J Heat Mass Transf 2017;110:113–31.
[23] Sun Y, Guan Z, Gurgenci H, Hooman K, Li X. Investigations on the influence of nozzle arrangement on the pre-cooling effect for the natural draft dry cooling tower. Appl Therm Eng 2018;130:979–96.
[24] Trabelsi SE, Qoaider L, Guizani A. Investigation of using molten salt as heat transfer fluid for dry cooled solar parabolic trough power plants under desert conditions. Energy Convers Manage 2018;156:253–63.
[25] Dai Y, Wang X, Li X, Guan Z, Dai Y. Preliminary analysis of direct and indirect heat rejection systems for a small sCO_2 Brayton cycle using an existing natural draft dry cooling tower. J Energy Eng 2018;144(2):04018005.
[26] Kröger DG. Air-cooled heat exchangers and cooling towers. PennWell Books; 2004.
[27] Terblanche J, Kröger D. Experimental evaluation of the aerodynamic inlet losses in cooling towers. S Afr Inst Mech Eng R&D J 1994;10(2):41–4.
[28] Lu Y. Small natural draft dry cooling towers for renewable power plants; 2015.
[29] Yoon SH, Kim JH, Hwang YW, Kim MS, Min K, Kim Y. Heat transfer and pressure drop characteristics during the in-tube cooling process of carbon dioxide in the supercritical region. Int J Refrig 2003;26(8):857–64.
[30] Churchill SW. Friction-factor equation spans all fluid-flow regimes. Chem Eng 1977;84(24):91–2.
[31] Lemmon EW, Huber ML, McLinden MO. NIST reference fluid thermodynamic and transport properties–REFPROP. ed: version; 2002.
[32] Bell KJ. Delaware method for shell-side design. New York: Taylor & Francis; 1988.
[33] Robinson KK, Briggs DE. Pressure drop of air flowing across triangular pitch banks of finned tubes. Chem Eng Prog Sympos Ser 1966;62(64):177–84.
[34] Briggs DE, Young EH. Convection heat transfer and pressure drop of air flowing across triangular pitch banks of finned tubes. Chem Eng Prog Sympos Ser 1963;59(41):1–10.